COMPARISON OF MIGRATION-BASED MICROSEISMIC LOCATION METHODS

L. Li, H. Chen, X. Wang, and D. Gajewski

email: *lei.li@uni-hamburg.de*

keywords: *microseismic monitoring, source location, migration, stacking*

ABSTRACT

Migration-based methods play an important role in microseismic source location, especially for surface monitoring with a large number of receivers. We compare three migration-based microseismic source location methods, namely, diffraction stacking, semblance-weighted stacking and cross-correlation stacking. The numerical results demonstrate the feasibility and robustness of migration-based methods for locating low signal-to-noise ratio microseismic events. Diffraction stacking and semblance-weighted stacking share the same stacking operator. The semblance-weighted waveforms can suppress the noise better, thus they result in higher imaging resolution. Cross-correlation stacking utilizes the interferometric migration operator and exhibits more reliable results when considering velocity uncertainty.

INTRODUCTION

Microseismic monitoring technology has become a research hotspot in passive seismology and unconventional oil and gas industry (Maxwell, 2014). The basic idea of microseismic monitoring is to monitor the fracture geometry based on the positions of seismic sources/acoustic emissions, so source location plays an essential role in the technology. In most cases, microseismicity has rather weak energy and exhibits very low signal-to-noise ratio (S/N), while the number of microseismic events is typically large. All these characteristics make it difficult for traditional traveltime inversion methods to locate microseismic events accurately and efficiently (Bardainne et al., 2009). In order to locate a large number of low S/N microseismic events reliably, migration-based methods have been proposed (Duncan, 2005). Migration-based methods utilize both kinematic information (e.g., traveltime) and dynamic information (e.g., amplitude) in the imaging process, and they can also be called beamforming or coherence scanning (Maxwell, 2014). These methods image and locate the sources by focusing the energy with certain types of imaging conditions, which are constructed by relations between the traveltime and the amplitude or energy contained in microseismic waveforms. Compared with classical traveltime inversion, migration-based methods have following advantages: (1) they need no phase picking and can avoid potential errors resulting from it; (2) due to the stacking process in imaging, they can detect more weak events in low S/N data ; (3) they can be directly united with source mechanism inversion and other reservoir characterization methods (Duncan and Eisner, 2010; Anikiev et al., 2014).

Due to the similarity of the characteristics of diffractors and seismic sources, most migration-based methods stack weak events along diffraction traveltime curves to enhance the location capabilities. For example, Kao and Shan (2004) stacked the absolute amplitudes to reconstruct the spatial and temporal distribution of the seismic sources. Gajewski et al. (2007) utilized the squared amplitudes to avoid polarization effects in surface arrays. Besides, the performances of some other waveform functions in diffraction stacking are also studied, such as short-term average to long-term average (STA/LTA) of the waveforms (Drew et al., 2005; Grigoli et al., 2013), semblance of the waveforms (Chambers et al., 2010), semblance-weighted waveforms (Eaton et al., 2011; Zhang and Zhang, 2013) and waveform envelopes (Gharti et al.,

2010). Another idea is to image microseismic sources by stacking the cross-correlograms (Grandi and Oates, 2009; Li et al., 2015). Microseismic waveforms from different receivers are cross-correlated and then stacked according to corresponding traveltime differences. This method is originated from seismic interferometric imaging and can also be called cross-correlation stacking/migration (Schuster et al., 2004). Recently, Trojanowski and Eisner (2017) compared several commonly used migration-based methods for surface microseismic monitoring. Their basic conclusions include: (1) the polarization correction could greatly enhance the imaging result; (2) semblance and cross-correlation based methods provided better location results than simple diffraction stacking, but they are more sensitive to velocity uncertainty.

In this work, we further study the location capability of three promising migration-based methods, namely, diffraction stacking, semblance-weighted stacking and cross-correlation stacking. Both P- and S-waves are considered in the imaging process, and no polarization correction is utilized for either of the methods. The basic principles of the three methods are introduced, followed by 2D and 3D numerical examples of surface monitoring. Absolute values, envelop values and squared values of waveforms can all handle the polarity issues at the expense of imaging resolution, but the latter can enhance the S/N and focus the source energy better by enlarging the differences between signals and noises. Numerical examples indicate that all the three migration-based methods can locate low S/N microseismic events accurately with a reliable velocity model. Moreover, compared with the diffraction stacking operator, the interferometric migration operator utilized in cross-correlation stacking is less sensitive to velocity uncertainty.

METHOD

In order to image subsurface sources, most migration-based location methods need to discretize the model into grids and calculate the traveltime table with the given velocity model. In this section, the basic principles of the three migration-based methods are introduced and analyzed. Although two or three particle velocity components are simulated in this study, the imaging process and the equations for all methods are conducted with the different components individually.

Diffraction stacking

Diffraction stacking is a commonly-used stacking method in exploration seismology, and it is the basis of classical Kirchhoff migration as well. A microseismic source can reasonably be treated as a diffraction point or point source. The basic imaging flow of diffraction stacking for microseismic source location includes two steps: calculation of the traveltime table and stacking the waveforms along the traveltime curves for all imaging points (see Figure 1a). For microseismic or passive seismic sources, the source excitation time is unknown and needs to be determined through repeating the stacking process for all possible excitation times (Gajewski et al., 2007; Zhebel et al., 2010). In order to eliminate the side effects of polarity changes, the squared values of original waveforms or cross-correlograms are utilized in this study. Compared with absolute values and envelop values, squared values can focus the source energy better and sacrifice less imaging resolution (The detailed comparison of different stacking methods with different waveform functions can be found in Appendix A). The diffraction stacking equation based on squared amplitudes reads as (Gajewski et al., 2007)

$$M_{DS}(\mathbf{x}, t_0) = \sum_{i=1}^{N} \left\{ \left[u_i(t^P_{\mathbf{x}i} + t_0)\right]^2 + \left[u_i(t^S_{\mathbf{x}i} + t_0)\right]^2 \right\}, \tag{1}$$

where $M_{DS}(\mathbf{x}, t_0)$ is the diffraction stacking value of position $\mathbf{x}$ at a specific assumed excitation time t_0, N is the number of receivers, u is the waveform amplitude of the considered component, e.g. the velocity component, $t^P_{\mathbf{x}i}$ and $t^S_{\mathbf{x}i}$ denote traveltimes from $\mathbf{x}$ to the i th receiver of the P- and S-wave, respectively. The imaging value $M_{DS}(\mathbf{x}, t_0)$ will reach its maximum when $\mathbf{x}$ coincides with the true source location and t_0 coincides with the true excitation time, provided that the model is correct.

Semblance-weighted stacking

Semblance is a coefficient of multichannel coherency between the receiver arrays, which is calculated by the energy ratio of the stack and the component traces (Neidell and Taner, 1971). Semblance can be used to

detect microseismic events (Tan et al., 2014), as well as image the source directly (Chambers et al., 2010). Instead of stacking the original waveforms or semblance values, semblance-weighted stacking utilizes the semblance-weighted waveforms, which can be obtained by (Zhang and Zhang, 2013)

$$S_n(t) = \frac{\sum_{w=-T_w/2}^{T_w/2} W\left(\sum_{i=1}^{N} u_{in}(\tau_i + t + w)\right)^2}{N \sum_{w=-T_w/2}^{T_w/2} W \sum_{i=1}^{N} u_{in}^2(\tau_i + t + w)}, \tag{2}$$

and

$$u_i^{Sem}(t) = S_n(t) \sum_{i=1}^{N} u_i(t), \tag{3}$$

where S_n is the semblance coefficient, n denotes a specific component, W is a certain type of window function, e.g., Gauss function, centered at the calculating time t, T_w is the time window, τ_i is the traveltime moveout of trace i with respect to a reference trace, which can be obtained by the cross-correlation function of two traces, u^{Sem} is the value of semblance-weighted waveform, which can effectively suppress noise by stacking similar P- or S-wave signals constructively and uncorrelated noise destructively. Similarly, squared values of semblance-weighted waveforms are used in the imaging process. The imaging equation is

$$M_{SS}(\mathbf{x}, t_0) = \sum_{i=1}^{N} \left\{ \left[u_i^{Sem}(t_{\mathbf{x}i}^P + t_0)\right]^2 + \left[u_i^{Sem}(t_{\mathbf{x}i}^S + t_0)\right]^2 \right\}, \tag{4}$$

where $M_{SS}(\mathbf{x}, t_0)$ is the semblance-weighted stacking value of position $\mathbf{x}$ at a specific assumed excitation time, t_0. The remaining parameters are the same as in equation (1).

Cross-correlation stacking

Cross-correlation stacking differs from traditional stacking methods, since it migrates and images the cross-correlograms instead of the original seismograms. Although diffraction stacking and semblance-weighted stacking utilize different waveform functions, they share the same diffraction stacking operator, while cross-correlation stacking uses the interferometric migration operator, which is based on the traveltime difference from the potential source to the receivers. The schematic diagram in Figure 1b shows the basic stacking process of cross-correlation stacking. The imaging equation is (Schuster et al., 2004; Li et al., 2015)

$$M_{CROSS}(\mathbf{x}) = \sum_{i,j=1}^{N} \left[\phi\left(i, j, \tau_{j\mathbf{x}} - \tau_{i\mathbf{x}}\right)\right]^2, \tag{5}$$

with

$$\tau_{j\mathbf{x}} - \tau_{i\mathbf{x}} = [(t_{iP} - t_{jS}), (t_{iP} - t_{jP}), (t_{iS} - t_{jS}), (t_{iS} - t_{jP})]|_{\mathbf{x}} = [\Delta t_{PS}, \Delta t_{PP}, \Delta t_{SS}, \Delta t_{SP}]|_{\mathbf{x}}, \tag{6}$$

where $M_{CROSS}(\mathbf{x})$ is the cross-correlation stacking value of position $\mathbf{x}$, ϕ is the cross-correlation function of two arbitrary traces i and j of the considered component, $\tau_{j\mathbf{x}} - \tau_{i\mathbf{x}}$ stands for the term of traveltime differences of direct waves, Δt_{PS} is the traveltime difference between P-wave and S-wave of two arbitrary traces, Δt_{PP}, Δt_{SS}, and Δt_{SP} have analogous meanings.

The cross-correlation stacking method studied here shares the same essence of cross-correlation technique as methods of Trojanowski and Eisner (2017) and Behzadi et al. (2015), although there are small differences in the stacking process. Note that the squared values of the cross-correlograms generated by the original waveforms are used in cross-correlation stacking. It is worth noting that the source excitation time t_0 is canceled in cross-correlation. Therefore, the method can save computation time by avoiding scanning for t_0 repeatedly, which also indicates t_0 cannot be directly determined by cross-correlation stacking. With the located source position, t_0 can be obtained by subtracting traveltime from the onset time.

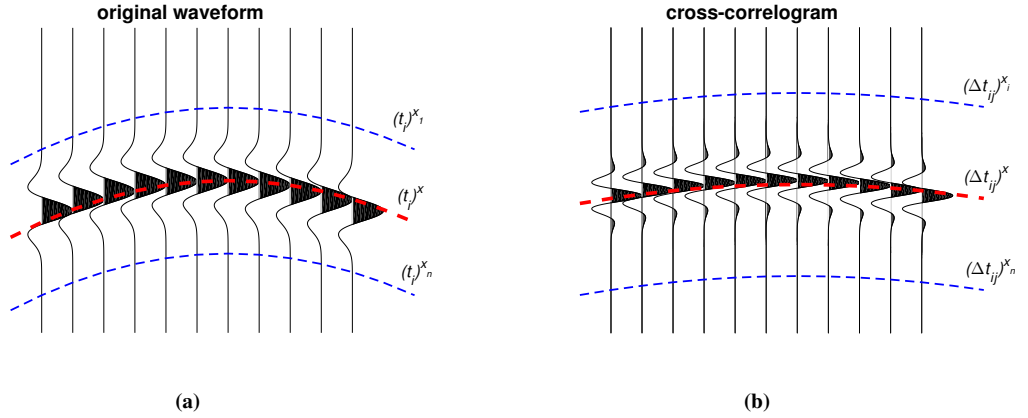

Figure 1: Schematic diagrams of the stacking process for the diffraction stacking operator (a) and the cross-correlation stacking operator (b).In both figures, $(t_i)^{\mathbf{x}}$ represents the traveltime from the potential source position $\mathbf{x}$ to the i th receiver. $(\Delta t_{ij})^{\mathbf{x}}$ represents the traveltime difference from $\mathbf{x}$ to a arbitrary receiver pair. When $\mathbf{x}$ coincides with the true source position, both stacking values reaches a maximum.

EXAMPLES

In this work, the staggered-grid finite-difference method (Vireux, 1986) is used to simulate microseismic records, and the eikonal solver package FDTIMES (Podvin and Lecomte, 1991) is used to calculate the traveltime of the first arrivals. Random noise is added to synthetic records to test the reliability of the methods. The S/N is calculated by $S/N = S_{RMS}/N_{RMS}$, where S_{RMS} and N_{RMS} are the root mean square (RMS) values of signal and noise, respectively. The S/N reduces to 1 dB after adding noise. The time spacing is 0.2 ms and the V_p/V_s ratio is set as 1.67. The source is simulated with a Ricker wavelet function with a main frequency of 50 Hz.

2D homogeneous model

In our first example, a 2D isotropic homogeneous model with a vertical point force are used to simulate elastic microseismic wavefields and records. The size of the model is 500 m $\times$ 400 m, the grid spacing in lateral and depth direction is 2 m. The P-wave velocity is 3000 m/s. The source is set at the center of the model. A surface receiver line with 51 equally-spaced receivers is set along horizontal direction at z = 0 m. The synthetic seismograms with noise are shown in Figure 2. We set the excitation time at 20 ms and search for it within a 40 ms long time window. The imaging results of the three migration-based methods based on equations (1), (4), and (5) are shown in Figure 3.

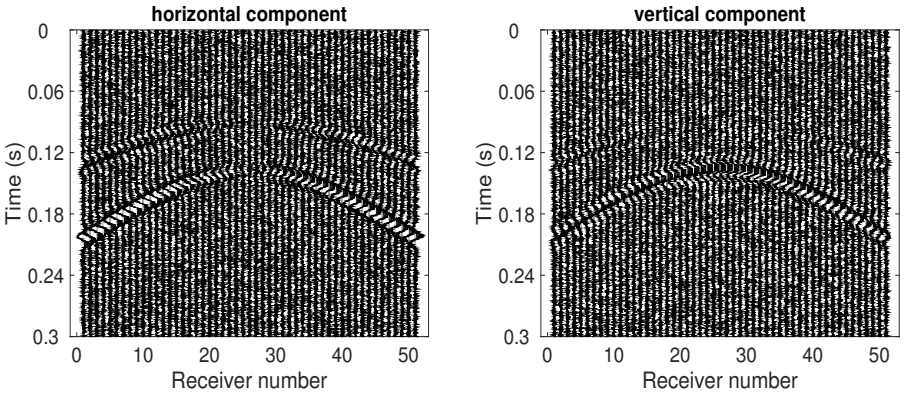

Figure 2: Synthetic microseismic records of the 2D homogeneous model.

All methods can suppress the noise effectively and locate the source accurately. The diffraction operator can determine the source excitation time simultaneously (Figure 3a and 3b), but it needs more calculation time.

2D complex fault model with velocity uncertainty

Velocity models obtained from seismic exploration and acoustic well-logging are generally not perfectly accurate, and they can deviate from the true subsurface model. In this section, a 2D complex fault model extracted from the 2D SEG/EAGE salt model (Schuster, 2009) is used to test migration-based methods. The size of the model is 500 m $\times$ 400 m and the source is placed at (250 m, 250 m). The remaining parameters are the same as in the homogeneous model in the previous subsection. The correct model and the corresponding imaging results of the vertical components are shown in Figure 4.

The velocity errors are generated by two approaches: (1) by adding a constant error to the velocity and (2) by smoothing the model to obtain a macro velocity model. In the first test, ± 5 % and ± 10 % errors are directly added to the velocity model. For the second test, the accurate velocity model is smoothed with a moving average window. Two different moving average windows are used, one is a size of 30 m in x-direction and 50 m in z-direction (referred to as macro model I, see Figure 5a), the other is 50 m in x-direction and 80 m in z-direction (referred to as macro model II, see Figure 5b). The location results of the vertical component are summarized in Table 1. It is visible that the location errors increase with velocity errors. Diffraction stacking and semblance-weighted stacking result in very similar characteristics of location errors since they utilize the same diffraction stacking operator. Compared with the traveltime itself, the traveltime difference is less sensitive to velocity errors. Therefore, there are fewer location errors for cross-correlation stacking, especially in the case of negative velocity errors. The macro velocity models result in smaller location errors since the smoothing process only changes the high frequency contents in the model (e.g., the fault interfaces), which have only low impact on traveltimes for relatively low-frequent microseismic waves.

Table 1: Absolute values of location errors. (unit: m)

Velocity Model	Diffraction Stacking	Semblance-weighted Stacking	Cross-correlation Stacking
+10 % error	28	30	26
+5 % error	12	12	16
correct model	4	6	4
-5 % error	22	22	2
-10 % error	38	38	10
macro model I	6	6	4
macro model II	8	6	2

3D horizontally layered model

Finally, a 3D horizontally layered model is used to simulate surface microseismic monitoring. The size of the model is 200 m $\times$ 200 m $\times$ 200 m, and the depths of the two considered interfaces are 50 m and 150 m, respectively. The P-wave velocities of three layers from the top to bottom are 2000 m/s, 2500 m/s, and 3000 m/s, respectively. The grid spacing is 2.5 m. The source is set at (125 m, 75 m, 100 m). A strike-slip source mechanism with a strike of 0°, dip of 90°, and rake of 0° is modeled, which is a common double-couple source in field microseismic data. For simplicity, the source excitation time is assumed to be known. Two orthogonal receiver lines with 21 equally-spaced receivers are placed along x-direction and y-direction, respectively. The intersection of two receiver lines is (100 m, 100m, 0 m). The synthetic microseismic records of the vertical component are shown in Figure 6. Although a star-array or rectangle-array is usually utilized in field surface monitoring, the simplified orthogonal receiver lines adopted here can also be used to verify the feasibility of the method. The imaging results of the vertical component for the three methods are shown in Figure 7. Since only two orthogonal arrays are used in this example, there

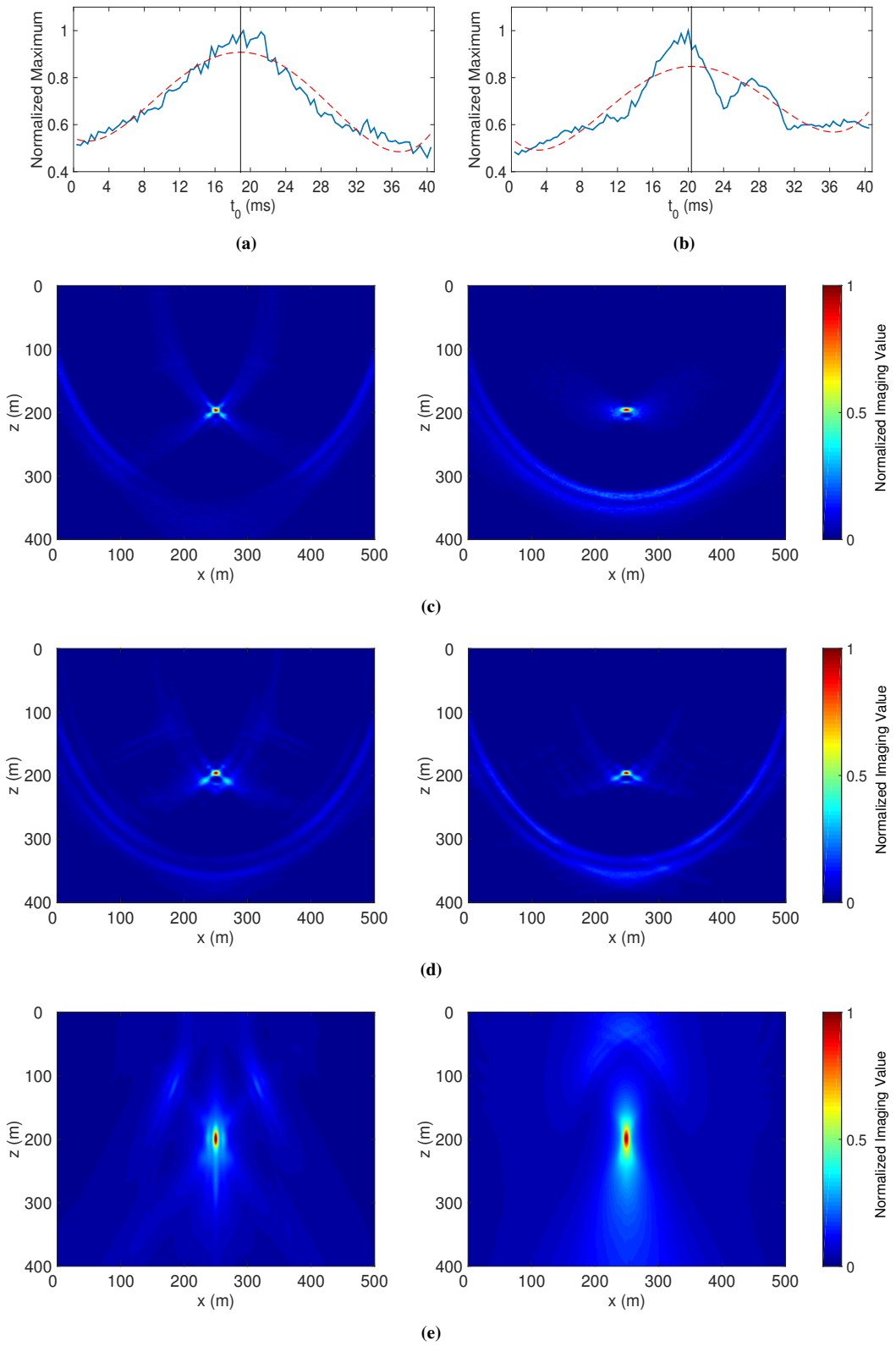

Figure 3: Imaging results of diffraction stacking (a, c), semblance-weighted stacking (b, d) and cross-correlation stacking (e). (a) and (b) are the normalized maximum imaging values corresponding to different assumed excitation times. The blue solid lines represent real imaging values of the horizontal component and the red dashed lines represent their polynomial fitted values, the global maximum of which correspond to the obtained excitation times. The left column of (c), (d), and (e) corresponds to the result of the horizontal component and the right corresponds to that of the vertical component.

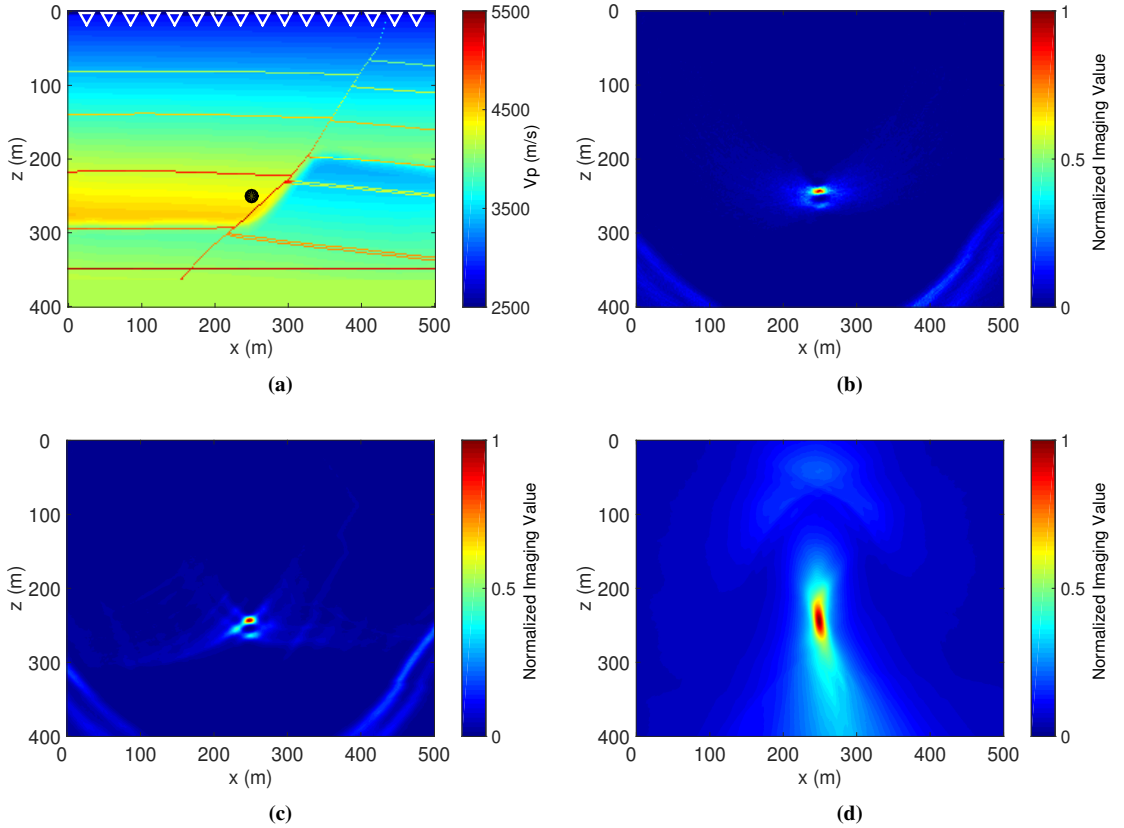

Figure 4: The 2D fault model and the imaging results. The white reversed triangles denote receivers and the black dot denotes the source. (b), (c), and (d) correspond to the imaging results of diffraction stacking, semblance-weighted stacking and cross-correlation stacking, respectively. Only results of vertical component are shown here.

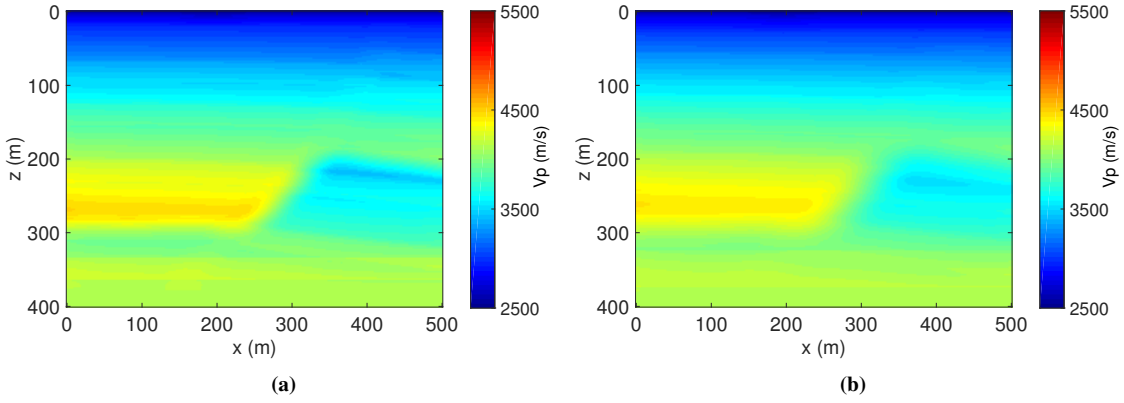

Figure 5: Smoothed fault velocity models: (a) macro model I, (b) macro model II. (See text for details)

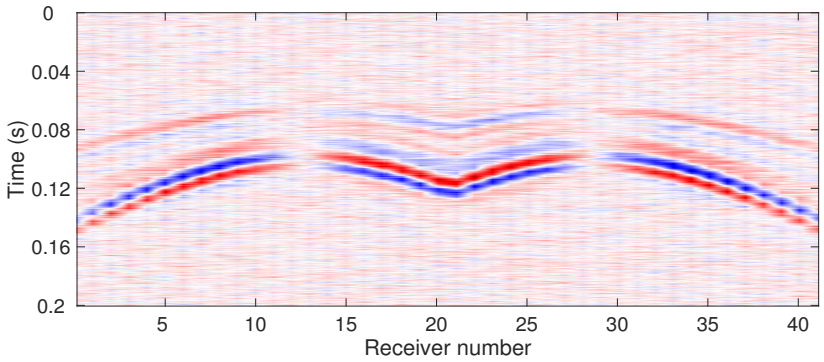

Figure 6: Synthetic microseismic records for two receiver lines on surface of the 3D horizontally layered model.

are obvious acquisition footprints for diffraction stacking and semblance-weighted stacking (see Figure 7a and 7b). The imaging result of cross-correlation stacking in Figure 7c is more accurate and convergent and has less acquisition footprints.

CONCLUSION AND OUTLOOK

In this work, we compared three migration-based microseismic location methods with 2D and 3D numerical examples. Under the condition of no polarization corrections, the stacking of squared values of waveforms has better imaging resolution than one of absolute values for all methods. Diffraction stacking and semblance-weighted stacking are based on the same diffraction stacking operator, where the latter stacks the semblance-weighted waveforms and results in a higher imaging resolution. Cross-correlation stacking utilizes the interferometric migration operator and exhibits less sensitivity to the velocity uncertainty.

The impact of velocity errors on the methods is just studied preliminarily in this work. Actual subsurface velocity models are usually complex and more factors, e.g., anisotropy, should be considered when accounting for velocity uncertainty. A joint source location and velocity inversion could be an alternative solution for better microseismic source inversion. In order to alleviate the effects of velocity errors on location, we are currently further researching the combination of migration-based methods and relative location approaches.

Source mechanism is another essential part for microseismic monitoring, by which we can obtain insight on the accurate growth process and connectivity of hydraulic fractures. Furthermore, knowledge of the source mechanism is also important for migration-based location methods. The location reliability can be highly improved with polarization corrections based on source mechanisms. Therefore, how to make use of the source mechanisms effectively in migration-based methods is another promising research point.

ACKNOWLEDGEMENTS

We thank the Applied Seismics Group Hamburg for continuous discussion and proof reading, especially Yujiang Xie, Leon Diekmann, Sergius Dell, Claudia Vanelle and Ekkehart Tessmer. We thank sponsors of the Wave Inversion Technology (WIT) Consortium. The work is also sponsored by National Natural Science Foundation of China (Nos. 11374322, 11574347). Lei Li is also grateful to China Scholarship Council (CSC) for partially funding this work.

REFERENCES

Anikiev, D., Valenta, J., Staněk, F., and Eisner, L. (2014). Joint location and source mechanism inversion of microseismic events: benchmarking on seismicity induced by hydraulic fracturing. *Geophysical Journal International*, 198:249–258.

Bardainne, T., Gaucher, E., Cerda, F., and Drapeau, D. (2009). Comparison of picking-based and

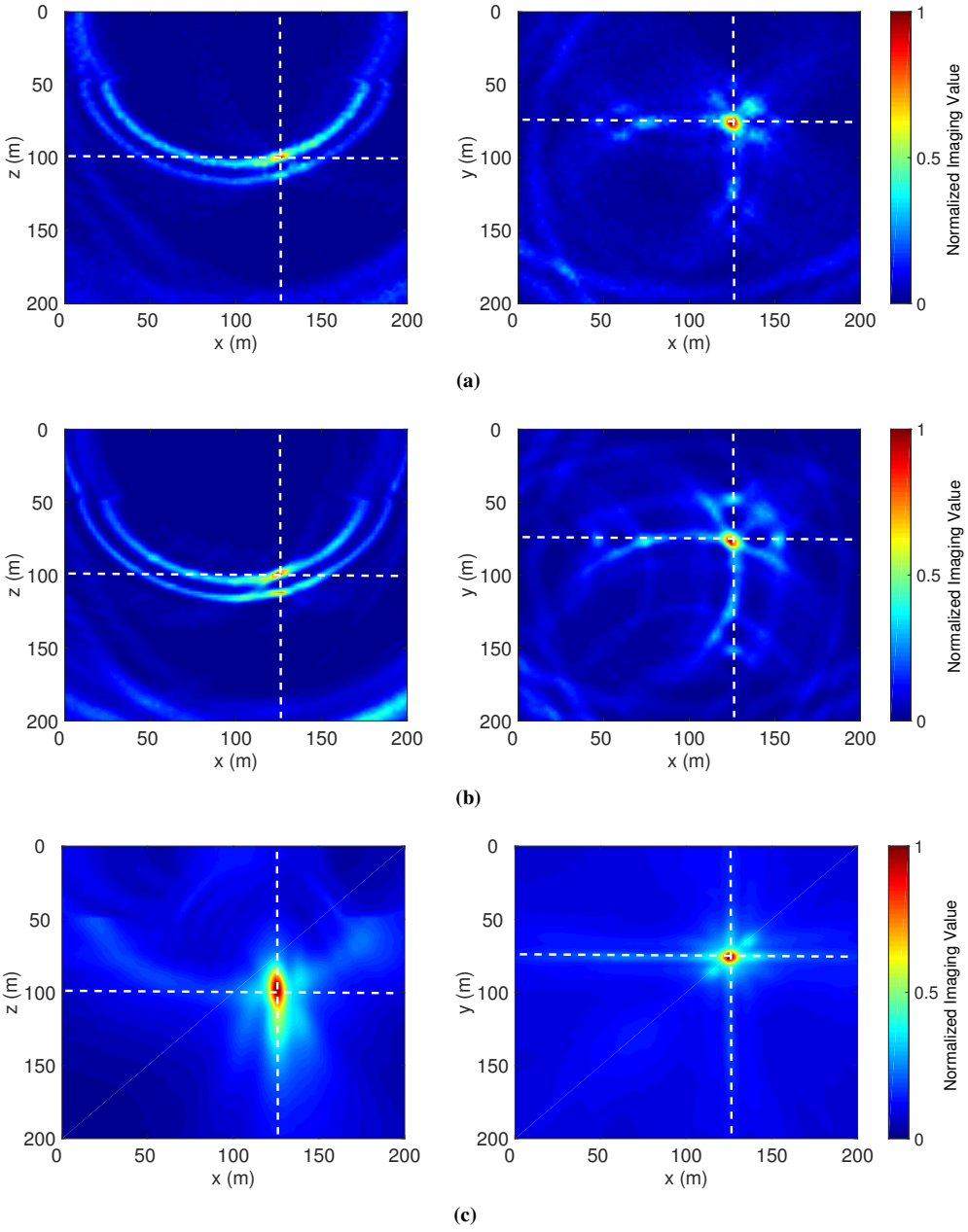

Figure 7: Imaging results of the vertical component for the three location methods. (a), (b), and (c) correspond to results of diffraction stacking, semblance-weighted stacking and cross-correlation stacking, respectively. The intersections of the white dashed lines indicate the true source positions.

waveform-based location methods of microseismic events: Application to a fracturing job. *SEG Technical Program Expanded Abstracts 2009*, pages 1547–1551.

Behzadi, M., Gajewski, D., and Vanelle, C. (2015). Seismic event localization based on cross-correlation stacking. *WIT Annual Report*, 18:217–230.

Chambers, K., Kendall, J.-M. B.-D. S., and Rueda, J. (2010). Testing the ability of surface arrays to monitor microseismic activity. *Geophysical Prospecting*, 58:821–830.

Drew, J., Leslei, D., Armstrong, P., and Michaud, G. (2005). Automated microseismic event detection and location by continuous spatial mapping. *2005 SPE Annual Technical Conference and Exhibition*, page Paper 95513.

Duncan, P. (2005). Is there a future for passive seismic? *First Break*, 23:111–115.

Duncan, P. and Eisner, L. (2010). Reservoir characterization using surface microseismic monitoring. *Geophysics*, 75:75A139–75A146.

Eaton, D. W., Akram, J., St-Onge, A., and Forouhideh, F. (2011). Determining microseismic event locations by semblance-weighted stacking. *2011 Canadian Society of Petroleum Geologists, Canadian Society of Exploration Geophysicists and Canadian Well Logging Society (CSPG CSEG CWLS) Convention*.

Gajewski, D., Anikiev, D., Kashtan, B., Tessmer, E., and Vanelle, C. (2007). Localization of seismic events by diffraction stacking. *SEG Technical Program Expanded Abstracts 2007*, pages 1287–1291.

Gharti, H. N., Oye, V., Roth, M., and Kühn, D. (2010). Automated microearthquake location using envelope stacking and robust global optimization. *Geophysics*, 75:MA27–MA46.

Grandi, S. and Oates, S. (2009). Microseismic event location by cross-correlation migration of surface array data for permanent reservoir monitoring. *71st EAGE Conference and Exhibition*, page X012.

Grigoli, F., Cesca, S., Vassallo, M., and Dahm, T. (2013). Automated seismic event location by traveltime stacking: An application to mining induced seismicity. *Seismological Research Letters*, 84:666–677.

Kao, H. and Shan, S. J. (2004). The source-scanning algorithm: Mapping the distribution of seismic sources in time and space. *Geophysical Journal International*, 157:589–594.

Li, L., Chen, H., and Wang, X. M. (2015). Weighted-elastic-wave interferometric imaging of microseismic source location. *Applied Geophysics*, 12:221–234.

Maxwell, S. C. (2014). *Microseismic Imaging of Hydraulic Fracturing*. Society of Exploration Geophysicists.

Neidell, N. S. and Taner, M. T. (1971). Semblance and other coherency measures for multichannel data. *Geophysics*, 36:482–497.

Podvin, P. and Lecomte, I. (1991). Finite difference computation of traveltimes in very contrasted velocity models: a massively parallel approach and its associated tools. *Geophysical Journal International*, 105:271–284.

Schuster, G. T. (2009). *Seismic Interferometry*. Cambridge University Press.

Schuster, G. T., Yu, J., and Sheng, J. (2004). Interferometric/daylight seismic imaging. *Geophysical Journal International*, 157:838–852.

Tan, Y., Yu, J., Feng, G., and He, C. (2014). A combined method for automatic microseismic event detection and arrival picking. *SEG Technical Program Expanded Abstracts 2014*, pages 2335–2340.

Trojanowski, J. and Eisner, L. (2017). Comparison of migration-based location and detection methods for microseismic events. *Geophysical Prospecting*, 65:47–63.

Vireux, J. (1986). P-SV wave propagation in heterogeneous media: velocity stress finite-difference method. *Geophysics*, 51:889–901.

Zhang, W. and Zhang, J. (2013). Microseismic migration by semblance-weighted stacking and interferometry. *SEG Technical Program Expanded Abstracts 2013*, pages 2045–2049.

Zhebel, O., Gajewski, D., and Vanelle, C. (2010). Localization of seismic events in 3D media by diffraction stacking. *SEG Technical Program Expanded Abstracts 2010*, pages 2181–2185.

APPENDIX A

Synthetic seismograms composed of 30 traces with aligned Ricker wavelets (the main frequency is 100 Hz) are used to test the performance of the three migration-based microseismic location methods. Random noise is added to the seismograms (S/N = 1 dB) (see Figure 8). In order to account for the effects of polarity changes, the polarities in the right half of the seismograms are inversed (Figure 8b). Stacking with the original waveforms with polarity changes results in unfocused or unreliable values (Figure 9b).

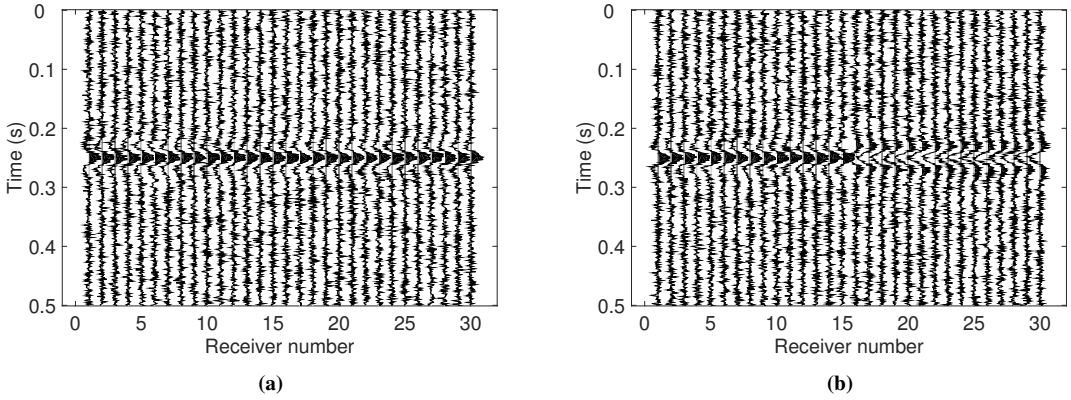

Figure 8: Synthetic seismogram of 30 traces with aligned Ricker wavelets: (a) without polarity changes, (b) with polarity changes.

Figure 10 shows the stacking results for the three migration-based methods with different waveforms and waveform functions. All three methods improve the S/N through stacking. Semblance-weighted stacking can suppress the noise and reconstruct the original wavelet best. Comparison of Figures 10a, 10b and 10c demonstrates that stacking with squared values of waveforms (see equation (1) and (4)) or cross-correlograms (see equation (5)) results in more focused curves than stacking with absolute values and envelop values. This result indicates that a higher imaging resolution can be obtained by stacking squared values rather than absolute values or envelop values (see Figure 11).

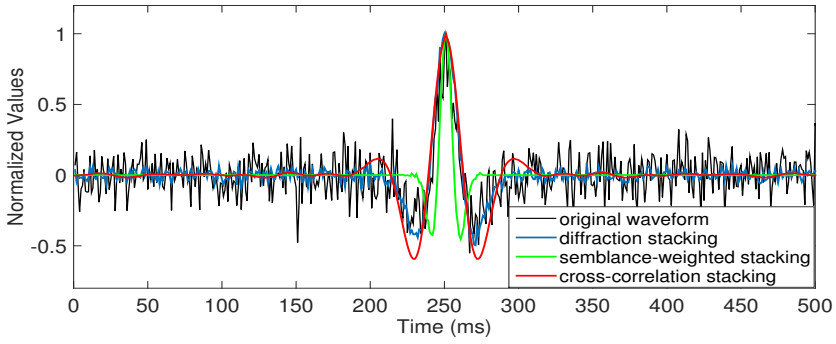

(a)

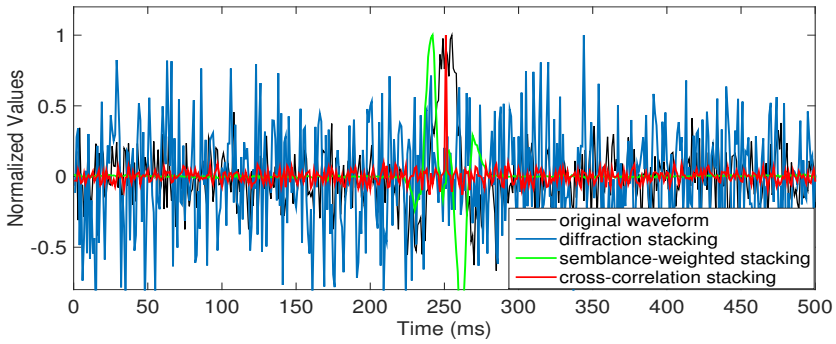

(b)

Figure 9: Stacking results using original waveforms. (a) is the result without polarity changes (see Figure 8a) and (b) is results with polarity changes (see Figure 8b).

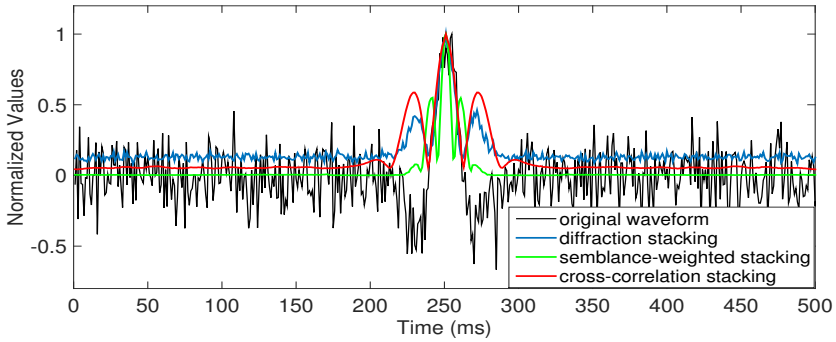

(a)

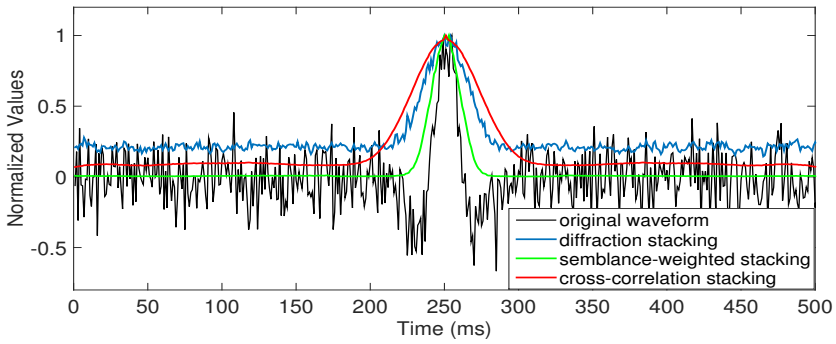

(b)

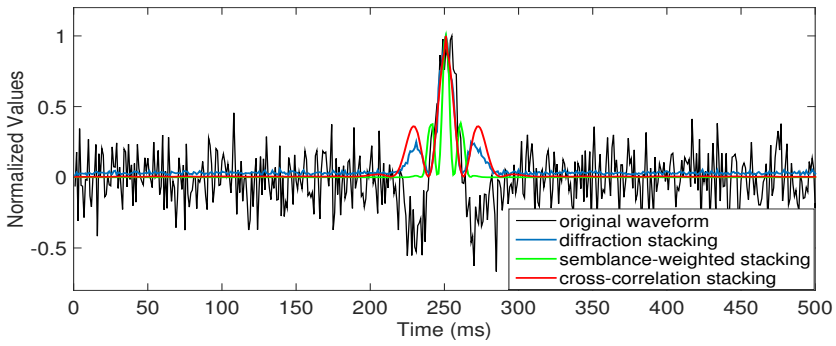

(c)

Figure 10: Stacking results for different stacking methods with different waveform functions. (a), (b), and (c) correspond to the results using absolute values, envelop values and squared values of original waveforms with polarity changes.

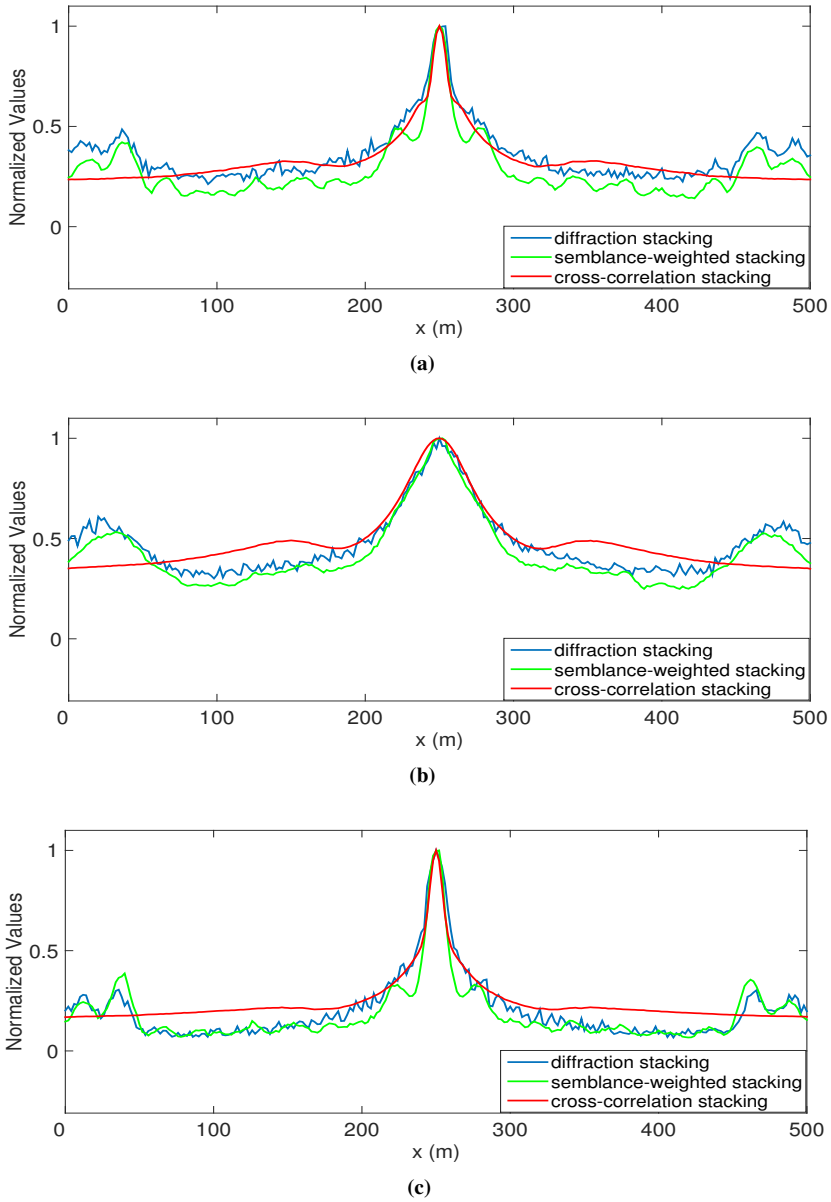

Figure 11: Comparison of horizontal imaging resolutions for different stacking methods with absolute values (a), envelop values (b), and squared values (c). The results are based on a 2D homogeneous model and the curves in (c) are extracted from z = 200 m in the right subfigures of Figures 3c, 3d, and 3e.